The Role of Spin for Kinetic Control of Recombination in Organic Photovoltaics

ARTICLE *in* NATURE · AUGUST 2013

Impact Factor: 41.46 · DOI: 10.1038/nature12339 · Source: PubMed

LETTER

doi:10.1038/nature12339

The role of spin in the kinetic control of recombination in organic photovoltaics

Akshay Rao[1], Philip C. Y. Chow[1], Simon Gélinas[1], Cody W. Schlenker[2], Chang-Zhi Li[3], Hin-Lap Yip[3], Alex K.-Y. Jen[2,3], David S. Ginger[2] & Richard H. Friend[1]

In biological complexes, cascade structures promote the spatial separation of photogenerated electrons and holes, preventing their recombination[1]. In contrast, the photogenerated excitons in organic photovoltaic cells are dissociated at a single donor–acceptor heterojunction formed within a de-mixed blend of the donor and acceptor semiconductors[2]. The nanoscale morphology and high charge densities give a high rate of electron–hole encounters, which should in principle result in the formation of spin-triplet excitons, as in organic light-emitting diodes[3]. Although organic photovoltaic cells would have poor quantum efficiencies if every encounter led to recombination, state-of-the-art examples nevertheless demonstrate near-unity quantum efficiency[4]. Here we show that this suppression of recombination arises through the interplay between spin, energetics and delocalization of electronic excitations in organic semiconductors. We use time-resolved spectroscopy to study a series of model high-efficiency polymer–fullerene systems in which the lowest-energy molecular triplet exciton (T_1) for the polymer is lower in energy than the intermolecular charge transfer state. We observe the formation of T_1 states following bimolecular recombination, indicating that encounters of spin-uncorrelated electrons and holes generate charge transfer states with both spin-singlet (^{1}CT) and spin-triplet (^{3}CT) characters. We show that the formation of triplet excitons can be the main loss mechanism in organic photovoltaic cells. But we also find that, even when energetically favoured, the relaxation of ^{3}CT states to T_1 states can be strongly suppressed by wavefunction delocalization, allowing for the dissociation of ^{3}CT states back to free charges, thereby reducing recombination and enhancing device performance. Our results point towards new design rules both for photoconversion systems, enabling the suppression of electron–hole recombination, and for organic light-emitting diodes, avoiding the formation of triplet excitons and enhancing fluorescence efficiency.

The key photophysical processes in an organic photovoltaic cell (OPV) are illustrated in Fig. 1a. In the first step, photogenerated excitons are dissociated by charge transfer across the donor–acceptor interface, leading to either long-range charge separation or the formation of bound interfacial charge transfer states[2] (CTSs). Such bound charge pairs then decay to the ground state by means of geminate recombination. Spin must be taken into account when considering CTSs because they can have either singlet (^{1}CT) or triplet (^{3}CT) spin character, which are almost degenerate in energy[5]. Dissociation of photogenerated singlet excitons leads to the formation of only ^{1}CT states, owing to spin conservation. In contrast, recombination of spin-uncorrelated charges, that is, bimolecular recombination, should lead to the formation of ^{1}CT and ^{3}CT states in a 1:3 ratio, according to spin statistics. Spin-singlet states can recombine to the ground state through either luminescence (which is slow for this intermolecular donor–acceptor process) or non-radiative decay[6]. For ^{3}CT states, decay to the ground state is spin-forbidden and, hence, both radiative and non-radiative processes are very slow. However, if the energy of the T_1 state is less than the ^{3}CT energy (as is required to maximize open circuit voltage, V_{OC}; refs 7, 8), then ^{3}CT can relax to T_1.

The most efficient OPV systems comprise nanoscale (<5 nm) domains of pure fullerene acceptor and domains of fullerene intimately mixed with a polymer donor[9,10]. These length scales are smaller than the Coulomb capture radius, r, in organic semiconductors ($k_BT = e^2/4\pi\varepsilon_0\varepsilon r$, where k_B is Boltzmann's constant, T is the temperature, e is the electron charge, and ε_0 and ε are respectively the vacuum and relative permittivities), which is ~16 nm at room temperature owing to the low dielectric constant of these materials[11] ($\varepsilon \approx 3$–4). This leads to a high rate of electron–hole encounters that could produce Coulombically bound CTSs. This model for recombination and the importance of spin statistics are well established in organic light-emitting diodes, where the formation of (non-luminescent) triplet excitons through bimolecular recombination is a major loss mechanism[3]. Efforts to overcome this problem have focused on the use of metal–organic complexes to induce spin–orbit coupling[12] and, more recently, on the use of low-exchange-energy materials that can promote intersystem crossing from T_1 to S_1 (ref. 13).

In contrast, for OPVs electron–hole encounters have been thought of as terminal recombination events[11,14,15], which, as noted above, is at odds with the high external quantum efficiencies (EQEs) demonstrated in empirically optimized systems[4]. Moreover, the roles of spin and the nature of the intermediate bound CTSs formed after electron–hole capture have not been explored. Here we demonstrate that the recombination of these bound states is mediated not only by energetics, but also by spin and delocalization, allowing for free charges to be reformed from these bound states and thus greatly suppressing recombination.

Figure 1b shows the structures of the two polymers and three fullerene derivatives used as electron donors and, respectively, acceptors in this study. $PC_{60}BM$ (phenyl-C_{60}-butyric acid methyl ester), $PC_{70}BM$ (phenyl-C_{70}-butyric acid methyl ester) and $IC_{60}MA$ (indene–C_{60} monoadduct, referred to as ICMA) are mono-substituted fullerene derivatives[16]. The lowest unoccupied molecular orbital of ICMA is raised by less than 0.1 eV in comparison with $PC_{60}BM$, whereas in $IC_{60}BA$ (indene–C_{60} bisadduct, referred to as ICBA), a bis-substituted derivative, the energy of the lowest unoccupied molecular orbital is raised by about 0.2 eV (refs 17, 18) The donor copolymer PIDT-PhanQ (poly(indacenodithiophene-co-phenanthro[9,10-b]quinoxaline)) was chosen for this study because in it the spectral signatures of charges (hole polarons) and triplets are considerably different[18,19]. As we explain below, this allows us to resolve temporally the interconversion between charges and triplets. It has been recently demonstrated that 1:3 blends of PIDT-PhanQ with $PC_{60}BM$ give excellent photovoltaic performance with internal quantum efficiencies >80% and power conversion efficiencies >4% (ref. 18). In contrast, blends with either ICMA or ICBA give lower performance with power conversion efficiencies of 2.9%. PCPDTBT (poly[2,6-(4,4-bis-(2-ethylhexyl)-4H-cyclopenta[2,1-b;3,

[1]Cavendish Laboratory, University of Cambridge, Cambridge CB3 0HE, UK. [2]Department of Chemistry, University of Washington, Seattle, Washington 98195-1700, USA. [3]Department of Materials Science & Engineering, University of Washington, Seattle, Washington 98195-2120, USA.

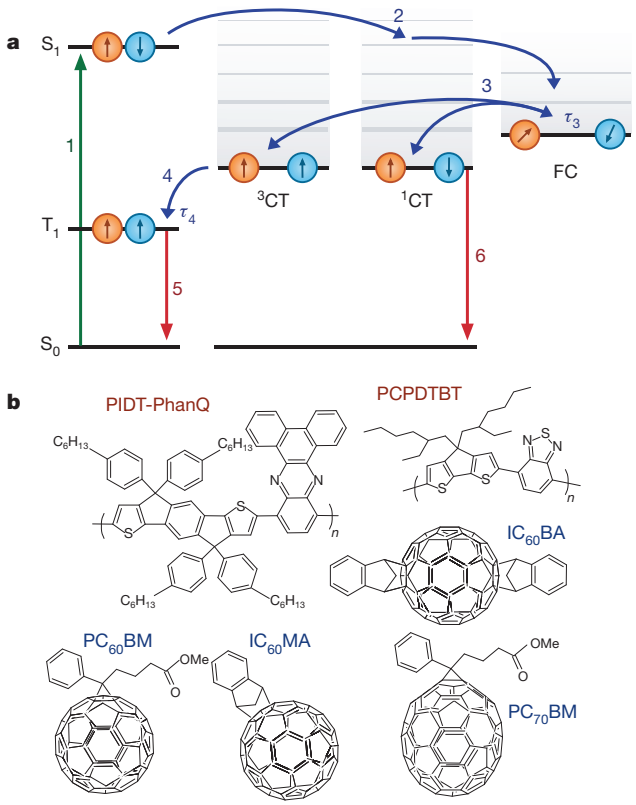

Figure 1 | Photophysical process in an OPV and molecular structures. **a**, State diagram representing the various photophysical processes in an OPV. Conversions between excited state species are shown in blue and recombination channels are shown in red. S_1 and T_1 are the lowest-energy singlet and triplet excitons, respectively. Here we define the CTS energy as the energy of the relaxed, Coulombically bound electron–hole pair across the heterojunction. Process 1: photoexcitation creates a singlet exciton. Process 2: the singlet exciton is ionized at a heterojunction, leading to the formation of ^{1}CT states that separate into free charges (FC) with high efficiency. Process 3: bimolecular recombination of electrons and holes leads to the formation of ^{1}CT and ^{3}CT states in a 1:3 ratio, as mandated by spin statistics. The ^{1}CT state can recombine to the ground state (process 6). Process 4: for the ^{3}CT state, recombination to the ground state is spin-forbidden, but relaxation to the T_1 state is energetically favourable. Process 5: once formed, triplet excitons can return to the ground state through an efficient triplet–charge annihilation channel. Under favourable conditions, as explained in the text, the time required for CTSs to reionize to free charges, τ_3 (process 3), is less than the time required for relaxation to T_1, τ_4 (process 4). Thus, CTSs are recycled back to free charges, leading to a suppression of recombination. **b**, Molecular structures of the donors and acceptors used in this study. Me, methyl.

4-b′]-dithiophene)-alt-4,7-(2,1,3-benzothiadiazole)]) is a widely studied low-bandgap polymer. Despite extensive research, the performance of PCPDTBT:PC_{70}BM blends remains modest, with EQE ≈ 50% (ref. 20). Blends with ICMA or ICBA have even lower performance. Absorption spectra, EQE and current density (*J*)–voltage (*V*) curves are provided in Supplementary Information.

For all the studied blends, the energy of the CTS is greater than that of T_1. For PIDT-PhanQ blends, the energies of the CTSs have been previously established using their weak photoluminescence and were found to be 1.31, 1.36 and 1.44 eV for PIDT-PhanQ:PC_{60}BM, PIDT-PhanQ:ICMA and PIDT-PhanQ:ICBA, respectively[18]. The energies of T_1 in PIDT-PhanQ, PCPDTBT and the fullerene derivatives have been established to be 1 (ref. 18), 1 (ref. 21) and 1.5 eV (ref. 22), respectively. The CTS energy of PCPDTBT:PC_{70}BM blends has previously been measured to be 1.2 eV (ref. 23). The CTS energies of PCPDTBT:ICMA and PCPDTBT:ICBA are thus greater than this. Therefore, the molecular triplet exciton of the donor polymer is the lowest-energy excited state for all the studied blends. We note that this is the standard configuration in the current generation of donor–acceptor systems, driven by the need to maximize V_{OC}, which mandates that the charge transfer level lie close to S_1 (refs 7, 8).

Here we investigate thin films of these blends using high-sensitivity transient absorption spectroscopy with a broad spectral and temporal range (Methods). Figure 2a shows the transient absorption spectra of a 1:3 PIDT-PhanQ:PC_{60}BM blend. A broad photoinduced absorption (PIA) feature is formed between the wavelengths 1,100 and 1,500 nm within the instrument response time (2 ns) and decays over several hundred nanoseconds without spectral evolution. The long lifetime of the signal and the fact that it is not observed in pristine films of PIDT-PhanQ (Supplementary Information) rules out PIA by singlet excitons. In contrast, efficient photogeneration of charge is expected in this blend and, thus, the PIA is assigned to charges (hole polarons) on the polymer. Figure 2b shows equivalent spectra for a PIDT-PhanQ:ICMA blend. Here, at the earliest times, the shape of the PIA is similar to that for PIDT-PhanQ:PC_{60}BM (Fig. 2a), but at later times we observe spectral evolution. Between 1,100 and 1,170 nm, the signal decays with time. However, between 1,300 and 1,500 nm the PIA increases for the first 50 ns. The spectrum is also seen to broaden and redshift. This spectral evolution is even more pronounced in the PIDT-PhanQ:ICBA blend shown in Fig. 2c. Thus, unlike the PIDT-PhanQ:PC_{60}BM spectrum, which shows no spectral evolution and is consistent with the decay of a single excited state, the PIDT-PhanQ:ICMA and PIDT-PhanQ:ICBA spectra suggest that a second excited state with a PIA overlapping the PIA of charges is being formed on timescales of tens to hundreds of nanoseconds.

Figure 2e compares the normalized kinetics of PIDT-PhanQ:PC_{60}BM and PIDT-PhanQ:ICBA blends. The PIDT-PhanQ:PC_{60}BM blend (circles) shows no difference between the kinetics of the 1,100–1,200-nm and 1,400–1,500-nm regions, supporting the presence of only one excited-state species. In contrast, for the PIDT-PhanQ:ICBA blend (squares), a large difference in the kinetics of the two regions is observed. The rise time of the low-energy region is much longer than for the higher-energy region, indicating the growth of a second long-lived excited state species on nanosecond timescales.

Figure 2f compares the normalized kinetics of the 1,400–1,500-nm region in PIDT-PhanQ:ICBA for different values of pulse fluence. A clear dependence on pulse fluence is observed, with rise times (to the signal maximum) as large as 80 ns. Similar fluence dependence for the rise time is not observed for the 1,100–1,200-nm region (Supplementary Information), with the signal maximum occurring within the rise time of the instrument. The rise time of the 1,400–1,500-nm region is also fluence dependent in PIDT-PhanQ:ICMA but not in PIDT-PhanQ:PC_{60}BM (Supplementary Information). This fluence dependence in ICBA and ICMA blends indicates that the second excited-state species growing in is formed by bimolecular processes.

The overlapping spectra of the excited states make the analysis of their kinetics difficult. To overcome this problem, we use a genetic algorithm[24] that allows us to extract the individual spectra and kinetics from the data set (Methods). Figure 2d shows the two spectra (solid lines) that the algorithm extracts from the PIDT-PhanQ:ICBA spectrum in Fig. 2c. The spectrum in blue is the charge (hole polaron) and the one in red is the triplet exciton on PIDT-PhanQ. These assignments are based on previous continuous-wave PIA experiments[18] as well as early-time transient absorption measurements (Supplementary Information).

From the spectra and kinetics presented in Fig. 2, we can now observe that charges are formed within the instrument response time (2 ns) in all blends. For the 1:3 PIDT-PhanQ:PCB_{60}M blend presented in Fig. 2a, charges then decay on a 1-μs timescale and no triplet formation is observed. For PIDT-PhanQ:ICMA and PIDT-PhanQ:ICBA, triplet excitons are formed through bimolecular recombination on nanosecond timescales before decaying.

Figure 3a, b shows the kinetics, at various fluences, extracted from the genetic-algorithm-based global analysis for PIDT-PhanQ:ICMA

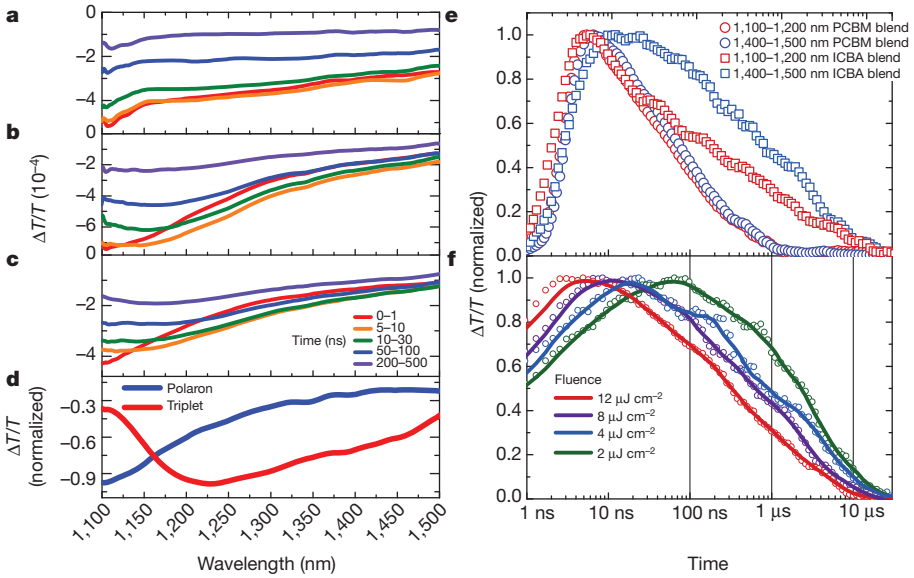

Figure 2 | Excited-state spectra and kinetics for PIDT-PhanQ blends. **a**–**c**, Temporal evolution of the transient absorption spectra for 1:3 blend ratios of PIDT-PhanQ:$PC_{60}BM$ (**a**), PIDT-PhanQ:ICMA (**b**) and PIDT-PhanQ:ICBA (**c**). Samples were excited with an excitation fluence of 8 μJ cm^{-2}. Temporal slices are averaged over the indicated time periods and smoothed. The $PC_{60}BM$ blend (**a**) shows only a slow decay with no spectral evolution. In contrast, the ICMA (**b**) and ICBA (**c**) blends show evolution up to 100 ns, indicating the growth of a new excited state species. **d**, The spectra extracted from the genetic algorithm analysis of the ICBA blend (**c**) showing the triplet and charge polaron spectra. **e**, Comparison of kinetics of PIDT-PhanQ:$PC_{60}BM$ (circles) and PIDT-PhanQ:ICBA (squares). Both the high-energy (red) and low-energy (blue) regions for PIDT-PhanQ:$PC_{60}BM$ decay on the same timescale, indicating the presence of only one excited-state species. In contrast, for PIDT-PhanQ:ICBA the regions have divergent kinetics, indicating the presence of multiple excited-state species. **f**, Fluence dependence of the low-energy region (1,400–1,500 nm) for PIDT-PhanQ:ICBA. The fluence-dependent growth of the feature demonstrates that the second excited-state species, triplets, are formed through bimolecular processes.

and PIDT-PhanQ:ICBA. The extracted kinetics clearly demonstrate that triplets grow in as charges decay. We consider that the primary decay channel for triplets is triplet–charge annihilation, owing to the high charge densities present, and model the time evolution of the system (Fig. 3a, b, solid lines) using the equation

$$\frac{dN_T}{dt} = -\alpha\frac{dp}{dt} - \beta N_T p \quad (1)$$

where p is the charge concentration, N_T is the triplet concentration, α is the fraction of decaying charges that form triplets and β is the rate constant for triplet–charge annihilation.

Values of β vary by a factor of two with fluence, and at a fluence of 2 μJ cm^{-2} for the PIDT-PhanQ:ICBA blend we obtain a value of 0.58 for α and a value of 2.2×10^{-10} cm^3 s^{-1} for β (Supplementary Information). This demonstrates that a large fraction of charges undergo bimolecular recombination, mediated by ^{3}CT, to form triplet excitons. Once formed, triplets are quickly quenched as a result of triplet–charge annihilation, as indicated by the high value of β. This is important: given sufficient time, triplets could be re-ionized through thermal excitation to CTSs. However, the presence of a strong triplet–charge annihilation channel means that recombination to triplets is a terminal loss and makes it a major loss pathway in OPVs.

We now turn to the question of whether the time taken for relaxation from ^{3}CT to T_1 (process 4 in Fig. 1a, with an associated timescale τ_4) is fast and, if not, whether there are competing processes for the decay of ^{3}CT. As noted earlier, for all PIDT-PhanQ:fullerene blends the charge transfer energy is greater than the T_1 energy, making relaxation from ^{3}CT to T_1 energetically favoured. However, for the more

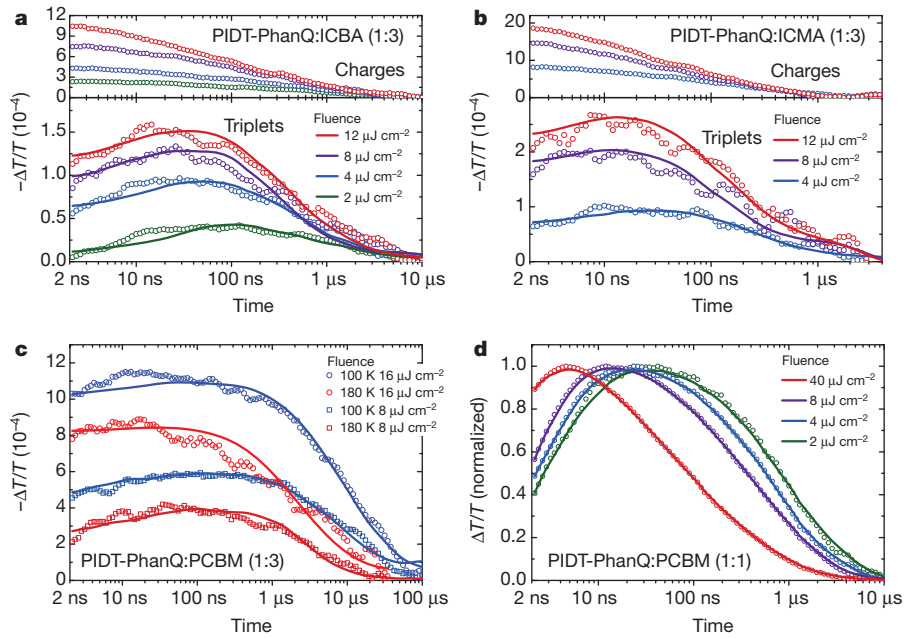

Figure 3 | Triplet and charge kinetics for PIDT-PhanQ blends. **a**, **b**, Charge and triplet dynamics for PIDT-PhanQ:ICBA (**a**) and PIDT-PhanQ:ICMA (**b**), extracted from the genetic algorithm analysis. Charges are formed within the instrument response time in all cases. The growth of triplets is fluence dependent, with a maximum population attained at later times for lower fluences. The solid lines are fits of the experimental data using the model described in the text. **c**, Temperature-dependent triplet dynamics (extracted using the genetic algorithm analysis) for a 1:3 PIDT-PhanQ:$PC_{60}BM$ sample. Open symbols show the experimental data and solid lines are fits using the model described in the text. The maximum triplet population is formed at later times at lower fluences and lower temperatures, consistent with a bimolecular-diffusion-dependent process. **d**, Room-temperature (297 K) fluence-dependent triplet dynamics (extracted using the genetic algorithm analysis) for a 1:1 PIDT-PhanQ:$PC_{60}BM$ blend spun from chloroform. In contrast to the 1:3 PIDT-PhanQ:$PC_{60}BM$ blend (Fig. 2a), this blend shows room-temperature triplet formation, which, as indicated by the fluence dependence, stems from bimolecular processes. Solid lines are guides to the eye.

efficient 1:3 PIDT-PhanQ:$PC_{60}BM$ blend, no triplet formation is observed at room temperature (Fig. 2a). But at low temperatures (<240 K), bimolecular triplet formation is observed in this blend (Fig. 3c; temperature-dependent kinetics of the raw data are provided in Supplementary Information). The solid lines are fits using the model described in equation (1). This result suggests that there is a thermally activated process that competes with relaxation to T_1. We consider this process to be the dissociation of ^{3}CT back to free charges. This is based on the fact that no other excited-state species are observed for this system (Fig. 2). Thus, at high temperatures (>240 K) the dissociation of ^{3}CT back to free charges (process 3 in Fig. 1a, with an associated timescale τ_3) out-competes relaxation of ^{3}CT to T_1; that is, $\tau_4 > \tau_3$. At lower temperatures, this dissociation process is suppressed, such that $\tau_4 < \tau_3$, leading to a build-up of triplet excitons (Fig. 3c).

The above result raises the question of why triplet formation is observed in ICBA and ICMA blends at room temperature but is out-competed by dissociation back to free charges in the 1:3 PIDT-PhanQ:$PC_{60}BM$ blend. As noted above, the charge transfer levels of the ICMA and $PC_{60}BM$ blends are within 50 meV of each other and, hence, a simple energetics argument is unlikely to explain this difference. Our previous work on CTSs formed at early times through the ionization of excitons at heterojunctions suggested that their dissociation was mediated by charge wavefunction delocalization[2]. We propose that the same mechanism is applicable to CTSs formed through bimolecular recombination. It is known that PCBM forms large aggregates efficiently, in contrast to other fullerenes, and that aggregation aids charge separation[25]. This effect is most probably due to delocalization of the electron wavefunction over the PCBM aggregates—fullerenes forming smaller aggregates would lead to more localized electron wavefunctions. This would imply that CTSs formed through recombination were more loosely bound in PIDT-PhanQ:$PC_{60}BM$ (1:3 blends) than in PIDT-PhanQ:ICMA and PIDT-PhanQ:ICBA and were thus more susceptible to dissociation back to free charges. To test this hypothesis, we study the recombination dynamics in a 1:1 PIDT-PhanQ:$PC_{60}BM$ blend spun from chloroform. The lower fullerene concentration and low-boiling-point solvent lead to a more intimate blend and arrest the growth of large fullerene aggregates. This is confirmed by grazing-incidence small-angle X-ray scattering measurements (Supplementary Information), which also show formation of smaller aggregates in the ICMA and ICBA blends than in the 1:3 PIDT-PhanQ:$PC_{60}BM$ blend. Bimolecular triplet formation is observed in the 1:1 PIDT-PhanQ:$PC_{60}BM$ blend (Fig. 3d), which shows the normalized fluence dependence of the triplets (raw data and charge dynamics are shown in Supplementary Information). Thus, by disrupting fullerene aggregation and, hence, charge delocalization, we make $\tau_4 < \tau_3$. This result confirms that delocalization has a crucial role in recombination.

To generalize the above results, we now study PCPDTBT blends. Figure 4a shows the evolution of the transient absorption spectrum of a 1:2 PCPDTBT:ICBA blend. A broad PIA feature between 1,175 and 1,550 nm is formed within the instrument response time (2 ns), and its peak blueshifts from 1,300 to 1,275 nm over tens of nanoseconds. A similar blueshift was observed in films of PCPDTBT:$PC_{70}BM$ and PCPDTBT:ICMA (Supplementary Information). The triplet spectrum extracted from a genetic algorithm analysis of the blends (Fig. 4b, solid red line) shows excellent agreement with the measured triplet spectrum in neat PCPDTBT (Fig. 4b, dashed red line; see Methods). The triplet peak at higher energy, with respect to the charge, explains the blueshifting of the transient absorption spectrum in Fig. 4a as triplets grow in.

Figure 4c shows the fluence dependence of the charge and triplet for a PCPDTBT:$PC_{70}BM$ film, similar to those shown in Fig. 3a, b. The solid lines are fits to the experimental data obtained using equation (1), and support the general applicability of the presented model. The result also explains why PCPDTBT blends have only modest EQEs[20], with recombination to triplets being a major loss mechanism even for the $PC_{70}BM$ blend.

On the basis of these results, we can now propose a new photophysical model of recombination in OPVs, summarized in Fig. 1a. Within working devices, the high charge densities present[26] (10^{16}–10^{17} cm^{-3}) lead to bimolecular electron–hole capture events forming CTSs with both spin-singlet and spin-triplet character, ^{1}CT and ^{3}CT. Recombination from ^{3}CT back to the ground state is spin-forbidden, but in most systems T_1 is lower in energy than CT, such that energetic relaxation to bound triplet excitons is favourable (with an associated time τ_4). The high charge densities then result in rapid quenching of these triplets. Thus, for most blends two recombination channels exist, one by means of triplets and the other through the radiative and non-radiative relaxation of the ^{1}CT states. However, as demonstrated in the PIDT-PhanQ:$PC_{60}BM$ system, when the acceptor is well ordered (encouraging wavefunction delocalization) the reionization of CTSs back to free charges (with an associated time τ_3) can occur faster than relaxation to T_1 ($\tau_4 > \tau_3$). In this case, the triplet recombination pathway is turned off, leaving only recombination through the singlet channel.

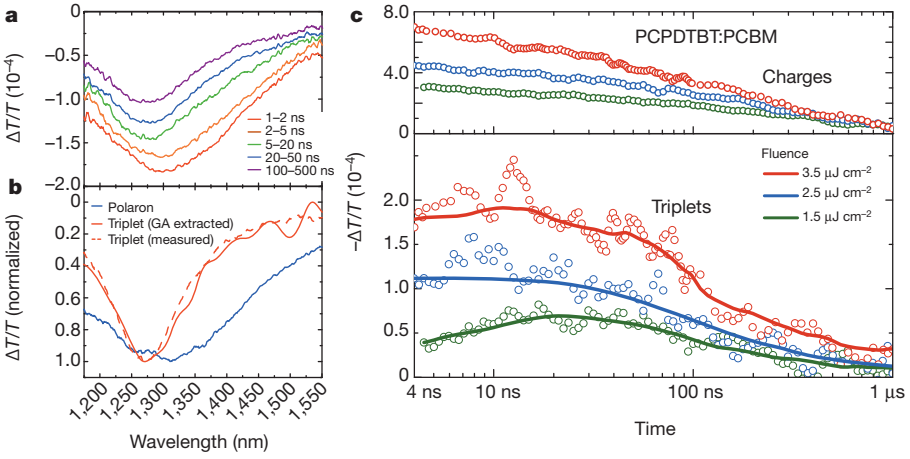

Figure 4 | Triplet and charge kinetics for PCPDTBT blends. **a**, Temporal evolution of the transient absorption spectrum for PCPDTBT:ICBA, excited with an excitation fluence of 2 μJ cm^{-2}. Temporal slices are averaged over the indicated time periods and smoothed. A blueshift of the spectra from a peak at 1,300 nm to 1,275 nm can be seen over the first 100 ns. **b**, Triplet spectrum extracted from the genetic algorithm (GA) analysis (solid red line) and that measured by doping a PCPDTBT thin film with a triplet sensitizer (dashed red line). The blue line shows the charge spectrum as measured 50 ps after photoexcitation, which is sufficient time for charge generation but not enough for triplet formation to begin. **c**, Charge and triplet dynamics (circles) for PCPDTBT:$PC_{70}BM$, extracted from the global genetic algorithm analysis, analogous to those shown in Fig. 3a, b. Charges are formed within the instrument response time in all cases. The growth of triplets is fluence dependent, with a maximum population attained at later times for lower fluences. The solid lines are fits of the experimental data using the model described in the text.

For working OPV devices, bimolecular recombination controls the shape of the J–V curve[26], with extraction of charges at the electrodes in competition with recombination. Recombination to triplets can proceed faster than extraction, and we observe triplet formation in working devices even under short-circuit conditions (Supplementary Information). As the voltage increases from short-circuit conditions towards V_{OC}, charge densities and extraction times increase, leading to higher bimolecular recombination losses. The film measurements here represent the case of V_{OC}, in which there is no extraction and recombination of all charges. We also note that any bimolecular recombination process that is non-radiative must reduce efficiency below the Shockley–Queisser limit[27], so avoidance of triplet formation is always desirable.

We note finally that the recombination current in OPVs is analogous to the injection current in organic light-emitting diodes, where electrons and holes with uncorrelated spins are injected from the electrode and recombine within the active layer. Recent efforts to minimize losses due to the formation of non-radiative triplets have focused on manipulating energetic levels such that triplet states are higher in energy than CTSs[27], or on finding systems with very low exchange energies[13]. However, these approaches can impose restrictive design criteria on materials and rely on inherently slow intersystem crossing from triplet to singlet. What we show here is that the introduction of weakly bound CTSs makes it possible to shut off recombination to non-radiative triplets, even when they are the lowest-energy excited state, and to achieve efficient recombination through the singlet channel. This insight opens a new route to high-efficiency fluorescent organic light-emitting diodes.

METHODS SUMMARY

PCPDTBT, ICMA and ICBA were obtained from 1-material, and $PC_{60}BM$ and $PC_{70}BM$ from Nano-C. PIDT-PhanQ was synthesized as described previously[18,19].

For the PIDT-PhanQ:fullerene thin-film samples, 1:3 polymer:fullerene blends (20 mg ml^{-1} in dichlorobenzene) were spun on fused-silica substrates. The PIDT-PhanQ:$PC_{60}BM$ thin film discussed in Fig. 3d was spun from a 1:1 blend (20 mg ml^{-1} in chloroform). For the PCPDTBT:fullerene thin-film samples, 1:2 polymer:fullerene blends (30 mg ml^{-1} in chlorobenzene) were spun on fused-silica substrates.

For transient absorption measurements, 90-fs pulses generated in a Ti:sapphire amplifier system (Spectra-Physics Solstice) operating at 1 kHz were used. The broadband probe beam was generated in a home-built non-collinear optical parametric amplifier. Pump pulses were generated using a frequency-doubled, q-switched Nd:YVO_4 laser (532 nm). Delay times from 1 ns to 100 μs were achieved by synchronizing the pump laser with the probe pulse using an electronic delay generator. Samples were measured in a dynamic vacuum ($<1 \times 10^{-5}$ mbar).

Full Methods and any associated references are available in the online version of the paper.

Received 4 February; accepted 29 May 2013.
Published online 7 August 2013.

1. Blankenship, R. E. *Molecular Mechanisms of Photosynthesis* ch. 7 (Blackwell Science, 2001).
2. Bakulin, A. A. *et al.* The role of driving energy and delocalized states for charge separation in organic semiconductors. *Science* **335,** 1340–1344 (2012).
3. Wallikewitz, B. H., Kabra, D., Gelinas, S. & Friend, R. H. Triplet dynamics in fluorescent polymer light-emitting diodes. *Phys. Rev. B* **85,** 045209 (2012).
4. Park, S. H. *et al.* Bulk heterojunction solar cells with internal quantum efficiency approaching 100%. *Nature Photon.* **3,** 297–302 (2009).
5. Hu, B., Yan, L. & Shao, M. Magnetic-field effects in organic semiconducting materials and devices. *Adv. Mater.* **21,** 1500–1516 (2009).
6. Morteani, A. C., Sreearunothai, P., Herz, L. M., Friend, R. H. & Silva, C. Exciton regeneration at polymeric semiconductor heterojunctions. *Phys. Rev. Lett.* **92,** 247402 (2004).
7. Veldman, D., Meskers, S. C. J. & Janssen, R. A. J. The energy of charge-transfer states in electron donor–acceptor blends: insight into the energy losses in organic solar cells. *Adv. Funct. Mater.* **19,** 1939–1948 (2009).
8. Vandewal, K., Tvingstedt, K., Gadisa, A., Inganas, O. & Manca, J. V. On the origin of the open-circuit voltage of polymer-fullerene solar cells. *Nature Mater.* **8,** 904–909 (2009).
9. Hammond, M. R. *et al.* Molecular order in high-efficiency polymer/fullerene bulk heterojunction solar cells. *ACS Nano* **5,** 8248–8257 (2011).
10. Lou, S. J. *et al.* Effects of additives on the morphology of solution phase aggregates formed by active layer components of high-efficiency organic solar cells. *J. Am. Chem. Soc.* **133,** 20661–20663 (2011).
11. Hilczer, M. & Tachiya, M. Unified theory of geminate and bulk electron-hole recombination in organic solar cells. *J. Phys. Chem. C* **114,** 6808–6813 (2010).
12. Baldo, M. A. *et al.* Highly efficient phosphorescent emission from organic electroluminescent devices. *Nature* **395,** 151–154 (1998).
13. Uoyama, H., Goushi, K., Shizu, K., Nomura, H. & Adachi, C. Highly efficient organic light-emitting diodes from delayed fluorescence. *Nature* **492,** 234–238 (2012).
14. Deibel, C., Baumann, A. & Dyakonov, V. Polaron recombination in pristine and annealed bulk heterojunction solar cells. *Appl. Phys. Lett.* **93,** 163303 (2008).
15. Koster, L. J. A., Mihailetchi, V. D. & Blom, P. W. M. Bimolecular recombination in polymer/fullerene bulk heterojunction solar cells. *Appl. Phys. Lett.* **88,** 052104 (2006).
16. Guangjin, Z., Youjun, H. & Yongfang, L. 6.5% efficiency of polymer solar cells based on poly(3-hexylthiophene) and indene-C_{60} bisadduct by device optimization. *Adv. Mater.* **22,** 4355–4358 (2010).
17. Hoke, E. T. *et al.* The role of electron affinity in determining whether fullerenes catalyze or inhibit photooxidation of polymers for solar cells. *Adv. Energy Mater.* **2,** 1351–1357 (2012).
18. Schlenker, C. W. *et al.* Polymer triplet energy levels need not limit photocurrent collection in organic solar cells. *J. Am. Chem. Soc.* **134,** 19661–19668 (2012).
19. Zhang, Y. *et al.* Indacenodithiophene and quinoxaline-based conjugated polymers for highly efficient polymer solar cells. *Chem. Mater.* **23,** 2289–2291 (2011).
20. Peet, J. *et al.* Efficiency enhancement in low-bandgap polymer solar cells by processing with alkane dithiols. *Nature Mater.* **6,** 497–500 (2007).
21. Di Nuzzo, D. *et al.* Improved film morphology reduces charge carrier recombination into the triplet excited state in a small bandgap polymer-fullerene photovoltaic cell. *Adv. Mater.* **22,** 4321–4324 (2010).
22. Soon, Y. W. *et al.* Energy versus electron transfer in organic solar cells: a comparison of the photophysics of two indenofluorene:fullerene blend films. *Chem. Sci.* **2,** 1111–1120 (2011).
23. Scharber, M. C. *et al.* Charge transfer excitons in low band gap polymer based solar cells and the role of processing additives. *Energy Environ. Sci.* **4,** 5077–5083 (2011).
24. Gélinas, S. *et al.* The binding energy of charge-transfer excitons localized at polymeric semiconductor heterojunctions. *J. Phys. Chem. C* **115,** 7114–7119 (2011).
25. Jamieson, F. C. *et al.* Fullerene crystallisation as a key driver of charge separation in polymer/fullerene bulk heterojunction solar cells. *Chem. Sci.* **3,** 485–492 (2012).
26. Credgington, D., Hamilton, R., Atienzar, P., Nelson, J. & Durrant, J. R. Non-geminate recombination as the primary determinant of open-circuit voltage in polythiophene:fullerene blend solar cells: an analysis of the influence of device processing conditions. *Adv. Funct. Mater.* **21,** 2744–2753 (2011).
27. Shockley, W. & Queisser, H. J. Detailed balance limit of efficiency of p-n junction solar cells. *J. Appl. Phys.* **32,** 510–519 (1961).

Supplementary Information is available in the online version of the paper.

Acknowledgements We thank N. Greenham for discussions. A.R. thanks Corpus Christi College, Cambridge for a Research Fellowship. S.G. thanks Fonds Québécois de Recherche sur la Nature et les Technologies for funding. This work is supported by the EPSRC and the Winton Programme for the Physics of Sustainability. C.W.S. was supported by the National Science Foundation (DMR-1215753). D.S.G., C.-Z.L., H.-L.Y. and A.K.-Y.J. acknowledge support from the Office of Naval Research (N00014-11-1-0300). Some of the work was done at the UW NanoTech User Facility, a member of the NSF National Nanotechnology Infrastructure Network. We thank J. Richards and D. Pozzo for performing grazing-incidence small-angle X-ray scattering measurements, S. Williams for transmission electron microscopy and G. Shao for help with atomic force microscopy measurements.

Author Contributions A.R. and P.C.Y.C. performed the time-resolved measurements. S.G. developed the numerical methods. A.R., P.C.Y.C. and S.G. analysed the data. C.W.S. and D.S.G. had the idea for the structural and steady-state spectroscopic measurements. C.-Z.L. synthesized PIDT-PhanQ. H.-L.Y. and A.K.-Y.J. had the idea for the molecular design of PIDT-PhanQ. R.H.F. supervised the work. A.R., P.C.Y.C., S.G. and R.H.F. wrote the manuscript. All authors commented on the manuscript.

Author Information Reprints and permissions information is available at www.nature.com/reprints. The authors declare no competing financial interests. Readers are welcome to comment on the online version of the paper. Correspondence and requests for materials should be addressed to R.H.F. (rhf10@cam.ac.uk).

METHODS

Transient absorption spectroscopy. In this technique, a pump pulse generates photoexcitations within the film, which are then studied at some later time using a broadband probe pulse. Although transient absorption has been widely used to study the photophysics of OPV blends, previous measurements have been severally limited by three factors: first, insufficient temporal range, typically a maximum of 2-ns delay between pump and probe; second, limited spectral range and a lack of broadband probes, which hinders the observation of dynamic interactions between excitations; and, last, insufficient sensitivity, which mandates the use of high excitation densities to create large signals. Here we overcome these problems by using broad temporal (up to 1 ms) and spectral windows (up to 1,500 nm) and high sensitivity (better than 5×10^{-6}). Although broad temporal[25] and spectral[28] windows have previously been achieved, all three requirements have not been met simultaneously before.

The temporal window is created by the use of an electrically delayed pump pulse and allows for the study of long-lived charges and triplet excitons. This was achieved by synchronizing the pump laser (a frequency-doubled, *q*-switched Nd:YVO_4 laser (532 nm) with 800-ps pulse width; AOT-YVO-25QSPX, Advanced Optical Technologies) with the probe pulse using an electronic delay generator (SRS DG535, Stanford Research Systems).

In conjugated polymers, local geometrical relaxation around charges (polaron formation) causes rearrangement of energy levels, bringing states into the semiconductor gap and giving rise to strong optical transitions in the range 700–1,500 nm (ref. 2). The absorption bands of singlet and triplet excitons are also found to lie in the near infrared, making a broadband spectral window necessary to track the evolution of the excited-state species. To generate these probe pulses, a portion of the output of a Ti:sapphire amplifier system (Spectra-Physics Solstice) operating at 1 kHz was used to pump a home-built non-collinear optical parametric amplifier modelled after ref. 29. The probe beam was split and a portion passed through a region of the sample not affected by the pump, so that laser fluctuations could be normalized. The probe and reference signals were dispersed in a spectrometer (Andor, Shamrock SR-303i) and detected using a pair of 16-bit, 512-pixel linear image sensors (Hamamatsu).

For short time measurements (pump–probe delay, <2 ns), the excitation pulses were generated by a TOPAS optical parametric amplifier (Light Conversion; 300-fs pulse width) seeded with a portion of the amplifier output, and the pump was delayed using a mechanical delay stage (Newport). Every second pump pulse was omitted electronically when using the *q*-switched source or, for short-time measurements, using a mechanical chopper. Data acquisition at 1 kHz was enabled by a custom-built board from Entwicklungsbüro Stresing. The differential transmission ($\Delta T/T$) was calculated after accumulating and averaging 1,000 pump-on and pump-off shots for each data point.

High stability of the probe beam, the use of a reference pulse to correct for shot-to-shot variation and the ability to read out every shot allows for a high signal-to-noise ratio. The high sensitivity of the experiment is essential as it allows us to probe the dynamics of systems when the excitation densities are similar to solar illumination conditions[26] (10^{16}–10^{17} excitations cm^{-3}; see Supplementary Information for calculation of excitation densities). At higher excitation densities, bimolecular exciton–exciton and exciton–charge annihilation processes can dominate, creating artefacts and making such measurements unreliable indicators of device operation under AM1.5G illumination[30].

All measurements were carried out under a dynamic vacuum ($<1 \times 10^{-5}$ mbar). Data obtained was then smoothed using a moving average filter in MATLAB. The step size of the filter was small to avoid losing spectral and temporal accuracy. For measurement of the triplet spectra of pristine PCPDTBT, the film was doped with an iridium complex that enhances the intersystem crossing rate, leading to a high triplet population. The measured triplet spectrum was found to be in good agreement with a previous measurement[28].

Numerical methods. To deconvolve the overlapping signatures of individual excited states and obtain their kinetics, we use numerical methods based on a genetic algorithm. The full details of this approach can be found elsewhere[24]. In summary, the algorithm starts by generating a large population of random spectra, which it then breeds into successive generations of offspring using a 'survival of the fittest' approach. Once the fitness stops improving with newer generations, the best spectra are returned as the optimized solution. For a given solution, the fitness is calculated as the inverse of the sum of squared residual, with a penalty added for non-physical results. The parents are selected using a tournament method with adaptive crossover and the offspring generated using a Gaussian-function mask (of random parameters) as the relative weight of each parent spectrum at a given wavelength.

28. Etzold, F. *et al.* The effect of solvent additives on morphology and excited-state dynamics in PCPDTBT:PCBM photovoltaic blends. *J. Am. Chem. Soc.* **134,** 10569–10583 (2012).
29. Cirmi, G. *et al.* Few-optical-cycle pulses in the near-infrared from a noncollinear optical parametric amplifier. *Opt. Lett.* **32,** 2396–2398 (2007).
30. Hodgkiss, J. M. *et al.* Exciton-charge annihilation in organic semiconductor films. *Adv. Funct. Mater.* **22,** 1567–1577 (2012).